

1 **Analytical and computer modelling of a thermo-mechanical vapour compression system for**
2 **space air conditioning in buildings**

3
4 Hussein A. Al Khiro* and Rabah Boukhanouf

5 Faculty of Engineering, University of Nottingham, Nottingham NG7 2RD, UK
6

7 **Abstract**

8 Air conditioning in buildings is essential for providing indoor thermal comfort, but it imposes a significant
9 electrical power load and carbon footprint, particularly when using traditional vapor compression systems.
10 This study investigates an innovative design and thermodynamic analysis of a cooling system that
11 integrates an ejector device into a basic vapour compression cycle and incorporates a thermally driven
12 second-stage compressor, forming the proposed thermo-mechanical vapor compression cooling system.
13 The second-stage compressor operates at constant volume, utilizing thermal energy from an external heat
14 source, such as a thermal solar collector. A MATLAB® model was developed to evaluate key energy
15 performance indices of the cycle for selected commercially available refrigerants, and the effect of external
16 heat source temperature and condenser temperature on the cooler's thermodynamic performance was
17 studied in detail. Results showed a marked reduction in mechanical compressor work using refrigerants
18 such as R161, R1270, R1234yf, and R1234zeE. For instance, the mechanical energy consumption was
19 reduced by 30.54%, and the Coefficient of Performance improved by 43.98% compared to the basic vapor
20 compression cycle, at a condenser temperature of 65°C and a superheated refrigerant temperature leaving
21 the thermal storage of 100°C using R1234yf. These findings indicate that the thermo-mechanical vapour
22 compression cooling system offers a promising solution for reducing energy consumption and carbon
23 emissions in buildings, particularly in hot climates.

24
25
26
27

*Corresponding author: Hussein Al-Khiro: ezxhk8@exmail.nottingham.ac.uk

28

29 **Keywords**

30 Vapor compression cycle, Ejector, constant volume thermal compression

31 **Nomenclature**

Variable	Description/unit
<i>COP</i>	Coefficient of performance
<i>h</i>	Refrigerant specific enthalpy (kJ/kg)
\dot{m}	Working fluid mass flow rate (kg/s)
<i>P</i>	Pressure (kPa)
<i>Q_{con}</i>	Condenser heat (W)
<i>Q_{ev}</i>	Cooling capacity (W)
<i>S</i>	Entropy (kJ/kg.K)
<i>T</i>	Temperature (°C)
<i>V</i>	Velocity (m/s)
<i>VCC</i>	Volumetric cooling capacity (KJ/m ³)
<i>W_{comp}</i>	Compressor work (W)
<i>x</i>	Vapour quality
Symbols	
η	Efficiency
μ	Entrainment ratio
<i>v</i>	Specific volume (m ³ /kg)
Subscripts	
<i>BVC</i>	Basic vapour compression cycle
<i>con</i>	Condenser
<i>diff</i>	Diffuser
<i>disc</i>	Discharge
<i>EVC</i>	Ejector vapour compression cycle
<i>evp</i>	Evaporator
<i>HS</i>	Heat Source
<i>interm</i>	Intermediate pressure
<i>is</i>	Isentropic
<i>mech</i>	Mechanical
<i>mix</i>	Mixing section
<i>mn</i>	Motive nozzle
<i>s</i>	Storage tank
<i>Sub</i>	Subcooled
<i>Sup</i>	Superheated
<i>sn</i>	Suction nozzle

32

33 **1. Introduction**

34 Modern buildings and high living standards depend on energy-intensive climate control systems to achieve

35 the required indoor thermal comfort. In warm climates, building operators prefer vapour compression-based

36 air conditioning (AC) for its convenience, availability, and easy control, providing a wide range of cooling
37 capacities from small residential window-mounted units for private flats to large centralized systems for
38 commercial buildings. Furthermore, vapor compression technology is endorsed as the ultimate solution for
39 decarbonising energy usage in buildings, even though it poses a significant environmental footprint through
40 the direct and indirect emission of greenhouse gases. According to the International Energy Agency
41 (International Energy Agency, 2018), the use of individual split AC units in the residential sector is projected
42 to surge from 850 million in 2016 to 3.7 billion by 2050. This growth is expected to increase electricity
43 demand from 6,200 GW to 23,000 GW, resulting in a doubling of CO₂ emissions from 1,135 million tons
44 (Mt) to 2,070 Mt.

45 In response to these concerns, numerous studies have focused on analytically and experimentally
46 enhancing the coefficient of performance (COP) of the basic vapour compression (BVC) systems and
47 optimising the cooling effect of refrigerants. One approach is increasing the degree of refrigerant subcooling
48 and superheating, which improves the cooling capacity. For example, (Rajendran et al., 2019) tested a
49 double-pipe suction line heat exchanger (SLHX) in a mobile BVC using R134a, resulting in an 8.2% to
50 10.5% reduction in power consumption and an 11.8% to 16.2% increase in COP. Furthermore, (Miran et
51 al., 2019) reported that using a dedicated mechanical sub-cooling technique improved COP by 36.1% using
52 refrigerant R170 (ethane), 30.74% for R744 (CO₂), and 26.48% for R744a (N₂O). It was also reported in
53 the literature the integration of thermoelectric coolers (TEC) for refrigerant sub-cooling in vapour
54 compression systems, though the technology is limited by low efficiency at high-temperature lifts,
55 (Aranguren et al., 2024) developed a computational model for an air-to-water propane (R290) heat pump
56 with thermoelectric subcooling, achieving a COP increase of 12.29% at for the evaporator and condenser
57 refrigerant discharge temperature of -20°C and 55°C respectively, while the seasonal coefficient of
58 performance (SCOP) improved by 9.98%. a similar study, (Kwan et al., 2020) found that integrating a TEC
59 device for heat exchange improved the cycle COP by a mere 5% as high thermal resistance limited the
60 heat transfer effectiveness.

61 Another promising approach is the phase change materials (PCM). (Riahi & Shafii, 2023) examined a water-
62 based PCM storage tank integrated with a vapour compression cycle for sub-cooling. During off-peak

63 operation, the refrigerant R134a is directed tank after the expansion valve, cooling the PCM and storing
64 cooling (charging), while on-peak operation the condenser refrigerant discharge is passed through the PCM
65 for sub-cooling, yielding a cooling capacity increase of 3.11% to 3.59%. However, this also resulted in a
66 COP reduction of 14.68% to 20.7%. In a similar follow-up study, (Riahi & Shafii, 2024) dynamically simulated
67 a PCM-integrated vapour compression cycle, however, during on-peak operation (discharging), the
68 refrigerant discharge the compressor is directed through the PCM store, lowering the condenser inlet
69 refrigerant temperature. This modification achieved a 23% reduction in daily electricity consumption
70 compared to the basic cycle.

71 In further developments to reduce mechanical work and energy losses, ejector devices have been used as
72 substitutes to conventional throttling devices. (Jain et al., 2024) evaluated a condenser split dual evaporator
73 vapour compression system for maintaining two evaporators at different temperatures by replacing the
74 throttling valve with an ejector, part went to the ejector while another expanded to the second evaporator.
75 This design reduced compressor work by 9.8% and improved the COP by 47.5% as the inlet of condenser
76 temperature decreased from 35°C to 27°C. Equally, (Chen et al., 2022) introduced a modified ejector-
77 enhanced dual-temperature refrigeration cycle using R290/R600a, in which the liquid-vapour refrigerant
78 separator was removed and a second recuperator was added, improving the cycle COP by 23%. (Cao et
79 al., 2022) analysed a two-stage evaporation cycle with the ejector as the primary expansion device, noting
80 a 22% COP increase and 49.5% reduction in exergy loss in the expansion process. (Zhang et al., 2020)
81 utilized the ejector for refrigerant expansion with a single-stage vapour compression cycle and low-pressure
82 refrigerant R1234yf, reporting a COP improvement of 7-20 %.

83 Furthermore, alternative low global warming potential (GWP) refrigerants were deployed both to enhance
84 the energy performance of the vapour compression technology and reduce the direct and indirect impact
85 on the environment(de Paula et al., 2020). simulated the performance of R290, R744, and R1234yf using
86 a basic vapour compression cycle, identifying that R290 achieved a COP comparable to R134a, with a
87 value of 2 under condenser and evaporator temperatures of 50°C and -3°C, respectively. Additionally, R290
88 was identified as a more environmentally friendly refrigerant, contributing to a 13% reduction in CO₂
89 emissions compared to R134a. (Al-Sayyab et al., 2022) explored the use of low-GWP refrigerants such as

90 R1234yf in a basic vapour compression cycle. Their study reported a 6% improvement in COP compared
91 to R134a, under condenser and evaporator temperatures of 60°C and 7.5°C, respectively. The work of
92 (Kulkarni et al., 2023) showed that R1234yf and R134a operate at similar levels of pressure and
93 temperature, though R1234yf shows a reduction in COP of up to 15%.

94 Integrating renewable energy sources like photovoltaic (PV) panels into vapor compression systems is
95 another way to reducing the environmental impact of these energy-intensive technology. (Zarei et al., 2022)
96 integrated a photovoltaic-thermal (PVT) system, ejector, and two-stage vapor compression refrigeration
97 cycle using R1234yf, R600a, and R290 to replace R134a. The electrical power generated by the PVT
98 collector powers the compressor motor, fans and water circulating pump, while the water outgoing the
99 collector serves to cool the condenser and sub-cool the refrigerant. This improved the COP by 8.23% when
100 R290 was used compared to the non-subcooled configuration. In a further development, (Yildiz et al., 2023)
101 employed a solar (PVT) module to generate hot water, which is passed through a heat exchanger that
102 interfaces with a BVC to superheat the refrigerant at the compressor suction port. The combined PVT-
103 vapour compression cycle achieved a COP 8.6% higher compared to BVC.

104 Several recent studies have investigated the benefit of adding a thermal compression stage to the BVC
105 using heat from waste heat sources or solar energy. For instance, (Elhelw et al., 2022) investigated the
106 performance of three cooling cycle configurations using different refrigerants. These configurations included
107 a standalone BVC, a modified BVC using partial thermal compression with an evacuated tube solar collector
108 (ETC), and a similar cycle with an added heat exchanger (HX) after the (ETC). The study evaluated R134a,
109 R152a, R290, R600a, and R1234yf as refrigerants. Their findings indicated that the combination of ETC
110 and HX achieved the most significant improvement, with a 20.3% COP increase with R290 as refrigerant.
111 (Bouraba et al., 2017) used heat generated from a solar thermal collector to increase R1234zeE refrigerant
112 vapour pressure at constant volume and reported that the COP was 20.45% higher than that of the basic
113 vapour compression, saving 16.98% of the compressor work. (Bellos et al., 2017) introduced a novel
114 approach by employing three vessels between the compressor and the condenser. The refrigerant inside
115 these vessels is heated by hot water, which is delivered through a solar thermal system via a suitable heat
116 exchanger. Results indicate that energy savings between 15% and 25% can be achieved when the

117 intermediate pressure following the mechanical compressor is set at 75% of the condenser pressure. (Abd-
118 Elhady et al., 2021) heated the refrigerant coming out of the compressor at constant volume to boost the
119 cooling rate of vapour compression cycle. It has been discovered that when the R134a refrigerant is heated
120 from 50 °C to 150 °C, the cooling power increases by 76.5%, to 200%, respectively.

121 The recent advancements in vapor compression systems design aiming to improve energy performance,
122 reported in literature predominantly address single modifications. However, the integration of thermal
123 compression and ejector technology into the vapour compression cycle presents a new area for research.
124 For example, alternative refrigerant vapour compression using constant volume processes presents
125 potential system design and integration with waste heat and renewables sources. For recovering energy
126 losses during expansion and reducing the mechanical compressor's workload. Furthermore, limited
127 research has examined system performance under high condenser temperatures, which is critical for
128 evaluating efficiency in hot climates.

129 **1.2 Innovation**

130 The reviewed literature unanimously supports that substituting the expansion valve of a basic vapour
131 compression system with an ejector leads to an increase in the COP. A similar finding has also been made
132 about the integration of thermally driven second-stage vapour compression, particularly when coupled with
133 low pressure refrigerants such as R1234yf and R1234zeE. Therefore, this study contributes to the
134 improvement of the energy efficiency of the vapour compression technology by integrating a dual refrigerant
135 compression process that combines mechanical vapor compression, assisted by an ejector, and a thermal
136 compression stage powered by external heat sources like solar energy forming a thermo-mechanical
137 vapour compression (TMVC) system. This design approach of the TMVC reduces the mechanical
138 compressor workload, increase the compressor suction pressure, and minimise the irreversibility of the
139 expansion process. The research method involves the formulation of a mathematical model and the
140 development of Matlab® computer code for the analysis of the ensuing thermodynamic cycle. Furthermore,
141 low Global Warming Potential (GWP) refrigerant such as R1270, R1234ze(E), R1234yf and R161 were
142 selected for energy performance comparison and potential energy savings in air conditioning applications.

143

144 2. Mechanical arrangement and operation of the proposed system

145 The thermo-mechanical vapour compression (TMVC) system consists of a conventional single-stage
146 vapour compression system in which the expansion valve is substituted with a liquid ejector and a second
147 stage refrigerant vapour compression at constant volume utilising thermal energy from an external heat
148 source such as a thermal solar collector. Fig. 1 shows a schematic diagram depicting the arrangement of
149 the principal components of the TMVC system. Like the single-stage traditional vapour compression system,
150 the superheated refrigerant vapour enters the mechanical compressor at point (1), where its pressure and
151 temperature undergo an isentropic compression process. In exiting the compressor, the refrigerant enters
152 the thermal compressor (the second vapor compression stage) at point (2), where it undergoes further
153 increase in pressure and temperature through a constant volume compression process. The thermal
154 compressor is made of a thermal heat source, a heat storage vessel, a heat exchanger, and a three-way
155 valve. The temperature-controlled three-way valve is installed in the refrigerant line between the mechanical
156 and thermal compressors. This valve directs the flow of refrigerant vapour through the thermal store or
157 bypasses it otherwise.

158 The primary refrigerant flow (motive flow) discharged from the condenser at point (4) enters the ejector
159 where it undergoes isentropic expansion through a convergent-divergent nozzle and exists at point (5). A
160 secondary flow is entrained into the suction chamber of the ejector (point 8, 9) and mixes with the primary
161 flow in the constant area of the ejector (point 10) before exiting the ejector diffuser as a mixture of liquid and
162 gas state at point (11). The refrigerant mixture is separated into vapour and liquid state in the separator
163 where the refrigerant directed to the mechanical compressor suction to repeat the cycle and the liquid leaves
164 at point (6) and is expanded through an expansion valve and enters the evaporator (point 7) for producing
165 cooling effect.

166 The p-h thermodynamic cycle of the system is presented in Fig. 2. The refrigerant vapour compression is
167 presented by the composite process 1-3 (isentropic mechanical compression 1-2 and constant volume
168 thermal compression 2-3). The constant pressure heat rejection is accomplished in the condenser (3-4).
169 The expansion through the ejector is isentropic process (4-5) and as it expands it entrains a secondary flow
170 perform cooling in the evaporator (7-8), increasing the basic vapour compression cycle (7'-8) cooling

171 capacity. It also worthwhile noting that the addition of a thermally driven constant volume compression
172 process, the vapour refrigerant enters the condenser at higher temperature than it would for a typical vapour
173 compression cooling cycle, which requires a larger condenser surface area.

174 Finally, to ensure the refrigerant enters the compressor superheated state, a suction line heat exchanger is
175 introduced.

176

177 **3. Mathematical model formulation**

178 The mathematical model of the thermodynamic cycle of TMVC system was conducted by applying the
179 fundamental theory of thermofluids to the basic vapour compression, ejector cycle and heat transfer from
180 the external heat source.

181 **3.1 Assumptions**

182 In developing the model, the following assumptions were considered:

- 183 • The system operates under fully established steady state conditions.
- 184 • Heat losses and pressure drop in the system's components are negligible.
- 185 • The refrigerant at suction line (point 1) and (point 8) is superheated and in the discharge line (point
186 4) is super cooled.
- 187 • The refrigerant in the ejector is considered as one-dimensional homogeneous equilibrium flow and
188 constant pressure mixing at point (10).
- 189 • The refrigerant and thermal store fluid temperature are equal, and the refrigerant is at the condenser
190 pressure.

191

192 **3.2 Refrigerant selection**

193 The design and energy efficiency of cooling systems are strongly linked to the type and thermophysical
194 properties of the refrigerant. (Kigali Amendment, 2016) has led to the phasing out and restrictions on the
195 use of certain refrigerants with high ozone depletion potential (ODP) and global warming potential (GWP).

196 In this work, the suitability of environmentally benign refrigerants such as R161, R1270, R1234ze(E), and
197 R1234yf was explored. Additionally, R134a and R410A are alluded to in this part to compare their
198 thermodynamic properties with other low GWP refrigerants. Table 1 presents the thermodynamic properties
199 of the considered refrigerants.

200

201 **3.3 Basic vapour compression cycle**

202 The ideal thermodynamic cycle of the basic vapour compression cycle is presented by 2'47'8 in Fig. 2.

203 The main specification parameters and the commonly used governing relationships of the cycle are given
204 in Table 2.

205

206 **3.4 Thermo-mechanical vapour compression thermodynamic cycle**

207 The analysis of the composite thermodynamic cycle of the TMVC system considers the properties of the
208 refrigerant at every stage of the cycle, as outlined in Table 3. The model proceeds from knowing the
209 properties of the liquid refrigerant in the discharge line of the condenser (Point 4).

210 At the mixing section of the ejector, point 10, the liquid and vapour phase refrigerant streams combine, and
211 the velocity of the mixture fluid can be calculated from the conservation of momentum equation as:

$$212 \quad \dot{m}_{con}V_{mn} + \dot{m}_{ev}V_{sn} = (\dot{m}_{con} + \dot{m}_{ev})V_{mix} \quad (36)$$

213 A mass flow rate ratio, r , of the motive fluid and total flow is given by:

$$214 \quad r = \frac{\dot{m}_{con}}{\dot{m}_{con} + \dot{m}_{ev}} \quad (37)$$

215 Therefore, the refrigerant flow mixture velocity in the ejector mixing area (point 10) can be written as:

$$216 \quad V_{mix} = \sqrt{\eta_{mix}(rV_{mn} + (1-r)V_{sn})} \quad (38)$$

217 An important characteristic of the ejector is the pressure lift which is a measure of how much the ejector
218 can "lift" the pressure from the suction side to the discharge side. This is expressed as:

$$219 \quad P_{lift} = \frac{P_{11}}{P_8} \quad (39)$$

220 **3.5 Energy performance parameters**

221 The main energy performance parameters of the TMVC system were evaluated as follows:

222 One of the important design parameters of the cooling system is to maximise the cooling capacity. This is
223 expressed as:

$$224 \quad Q_{ev, TMVC} = \dot{m}_{ev}(T_8 - T_7) \quad (40)$$

225 Equally important is to minimise the mechanical work required by the mechanical compressor to perform
226 refrigerant vapour compression in the first stage. This is determined as:

$$227 \quad W_{comp, TMVC} = \frac{\dot{m}_{con}(h_{2, is} - h_1)}{\eta_{is} \eta_{mech}} \quad (41)$$

228 where the compressor Isentropic efficiency is expressed by (Brunin et al., 1997):

$$229 \quad \eta_{is} = 0.874 - 0.0135 \frac{P_{disc}}{P_{suc}} \quad (42)$$

230 The refrigerant vapour compression in the second stage is accomplished by adding heat from an external
231 heat source. The amount of heat supplied can be calculated as:

$$232 \quad Q_{HS} = \dot{m}_{con}(h_3 - h_2) \quad (43)$$

233 From the energy conservation law, the total heat rejected in the condenser is the sum of the heat transferred
234 in the evaporator, the mechanical energy supplied in the mechanical compressor and thermal energy
235 supplied in the thermal compressor. This is determined from the following:

$$236 \quad Q_{con, TMVC} = \dot{m}_{con}(h_3 - h_4) \quad (44)$$

237 The mechanical coefficient of performance (COP) of the cycle is then determined as:

$$238 \quad COP_{TMVC} = \frac{Q_{ev, TMVC}}{W_{comp, TMVC}} \quad (45)$$

239 The improvement in thermal performance of the TMVC compared to BVC, can be expressed by the increase
 240 in COP as follows:

$$241 \quad COP_{imp,mech} = \frac{COP_{TMVC} - COP_{BVC}}{COP_{BVC}} \quad (46)$$

242 Similarly, the percentage of energy saved by the TMVC system compared to the BVC can be calculated as
 243 follows:

$$244 \quad ES = \frac{W_{comp, TMVC} - W_{comp, BVC}}{W_{comp, BVC}} \quad (47)$$

245 The improvement in energy performance of the TMVC system however is achieved at the cost of increased
 246 heat rejected in the condenser. This is given as:

$$247 \quad Q_{augmentation} = \frac{Q_{con, TMVC} - Q_{con, BVC}}{Q_{con, BVC}} \quad (48)$$

248 Finally, the compression ratio enhancement can be calculated by using below equation:

$$249 \quad CR_{enhancement} = \frac{\left(\frac{P_2}{P_1}\right)_{TMVC} - \left(\frac{P_2'}{P_8}\right)_{BVC}}{\left(\frac{P_2'}{P_8}\right)_{BVC}} \quad (49)$$

250

251 **4. Research Method**

252 A flow chart of the computer algorithm for the TMVC thermodynamic cycle is presented in Fig. 3. The
 253 algorithm comprises the basic vapour compression cycle, the basic cycle with the integration of an ejector
 254 device, and the complete TMVC system, which includes a thermal compressor supported by an external
 255 heat source. The mathematical model defined by equations (1) to (49) and associated initial design
 256 parameters are then solved iteratively in Matlab® to evaluate the main energy performance parameters of
 257 the TMVC and to quantify the improvement achieved compared to the basic vapour compression cycle. In
 258 this study, the performance enhancement of the TMVC was computed for the temperatures of the
 259 superheated refrigerant leaving the thermal store range from 75 to 100°C, with temperature increments,
 260 ΔT_s , of 1°C. Similarly, the effect of the condenser temperature was assessed for temperatures ranging from
 261 50 to 65°C, with increments, ΔT_{con} , of 5°C. The convergence of the computational model of the ejector

262 vapour compression cycle was attained when the value of the refrigerant flow ratio, r , approached the
263 refrigerant vapor quality, x_5 , (i.e., $|x_5-r| \leq \epsilon$) across the defined range of condenser and thermal store
264 temperatures.

265

266 **4.1 Model validation**

267 The computational modelling of the TMVC thermodynamic cycle was carried out using Matlab® software
268 linked to CoolProp database version 6.4.3 (Bell et al., 2014) for the retrieval of the thermophysical properties
269 of the refrigerant thermodynamic states. The accuracy of the basic vapour compression cycle with an ejector
270 device was verified by comparing the computational model results with those presented by (Li et al., 2014).
271 In this comparative analysis, analogous design conditions were selected, including $T_{con}= 40\text{ }^\circ\text{C}$, $T_{evp}= 5\text{ }^\circ\text{C}$,
272 $\eta_{mn} = \eta_{sn} = \eta_{dn} = 0.85$ and $\eta_{ms} = 0.95$ and refrigerant R1234yf. The performance of the system was then
273 evaluated in terms of COP and COP improvement, considering a pressure drop variation from 5 to 50 kPa
274 through the ejector nozzle. Fig. 4 illustrates that both the trend and values of COP and improvement of COP
275 obtained in this study closely align with those reported by (Li et al., 2014).

276 Furthermore, the computed COP of the integrated ejector and vapour compression cycle (EVC) was
277 compared with the experimental findings conducted by (Ersoy & Bilir Sag, 2014), as listed in table 4. It shows
278 that there is a good agreement between the computed COP and the experimental results.

279 A further validation of the computer model results was conduct against the experimental work of (Elhelw et
280 al., 2022) where the authors presented the results of a single-stage vapor compression cycle integrated
281 with an evacuated tube solar collector, as detailed in Table 5. The enthalpy and evaporator pressure
282 deviations were relatively small. In contrast, higher deviations at the mechanical compressor discharge,
283 thermal compressor inlet, and condenser pressure were attributed to model simplifications, such as
284 neglecting pressure losses in the heat exchangers. The experimental pressure accuracy of ± 0.15 bar may
285 have also contributed. The validation confirms the model's reliability within acceptable limits despite these
286 factors.

287

288 **5. Results and discussion**

289 To evaluate the effect of the refrigerant type, the energy performance indices of the TMVC were established
290 and compared against the basic vapour compression cycle. Table 6 shows the main parameters used in
291 this computer model.

292 **5.1 Effect of the type of refrigerant**

293 The choice of refrigerant in vapour compression systems influences the operating temperatures and
294 pressures of the cycle, thereby impacting the power demand and cooling capacity. To select a suitable
295 refrigerant from the list of refrigerants given in Table 1, the thermodynamic performance analysis of a basic
296 vapour compression refrigeration cycle was performed. In this analysis, the condenser and evaporator
297 temperatures were set at 65° C and 5°C, respectively. The analysis results are recapitulated in Table 7, which
298 shows that the low GWP refrigerants R1234yf and R1234ze(E) have the lowest compressor discharge
299 temperatures when compared to the critical temperatures of the respective refrigerants. Similarly, it was
300 found that the thermodynamic cycle performance parameters such as the compressor power, condenser
301 heat rejection rate and COP of refrigerants R1234ze and R123fy are not dissimilar to those of other refrigerants.
302 This further makes these two refrigerants suitable for the proposed TMVC system.

303 **5.2 Thermal performance analysis**

304 The energy performance of the proposed TMVC system was analysed under varying operating
305 conditions. The results highlight the influence of thermal store temperature on key performance
306 metrics, including COP, compressor mechanical work, and heat transfer in the condenser. The
307 following sections detail these effects for different refrigerants, emphasizing the system's
308 adaptability to high ambient temperature environments and energy-saving potential.

309 **5.2.1 Effect of thermal store temperature on the coefficient of performance**

310 The temperature of the superheated refrigerant vapour discharged from the compressor is increased in the
311 second stage (thermal compression) by the external heat source. The temperature of the refrigerant exiting
312 the thermal compression stage has a direct impact on the TMVC cycle COP. This is illustrated in Fig. 5(a)

313 to (d), where increasing the superheated refrigerant temperature from 75 to 100° C resulted in an increase
314 in the COP of the TMVC system for all refrigerants considered. As shown in Fig. 5(a) and (b), using R1234yf
315 and R1234zeE improved cycle COP by 44% and 34%, respectively, when the discharge refrigerant
316 temperature was kept at 100° C and the condenser temperature at 65° C. Equally, increasing the condenser
317 temperature from 50 to 65° C resulted in a minimal increase in COP due to the rise in the ejector pressure
318 lift ratio (p_{11}/p_8), which is consistent with the findings of (Sarkar, 2010). This indicates the suitability of the
319 TMVC for operation in a high ambient temperature environment. In contrast, at a condenser temperature
320 of 65°C, refrigerants R1270 and R161 would require a thermal compression stage temperature of 85 to
321 94°C to have any improvement of the system COP. Nevertheless, at discharge temperature of 100°C and
322 condenser temperature of 65°C, R1270 and R161 improved the cycle COP by 31% and 20%, respectively,
323 as illustrated in Fig. 5(c) and (d). The high COP improvement using R1234yf compared to R1234zeE, R161,
324 and R1270 is mainly the result of its lower discharge temperature relative to its critical temperature. This
325 allows a higher heat transfer rate during the constant volume thermal compression stage in the thermal
326 store.

327 **5.2.2 Effect of thermal store temperature on compressor mechanical work**

328 The TMVC system has two positive effects: the ejector increases pressure lift, which raises the compressor
329 suction pressure, and it increases the superheated refrigerant vapour temperature in the thermal store,
330 lowering the compressor discharge pressure, as the cycle's compression process occurs primarily in the
331 thermal compressor. As shown in Fig. 6, these factors reduce compressor work and increase energy
332 savings compared to a basic vapour compression cycle with all refrigerants.

333 It was also observed that the refrigerants with low discharge temperatures (Fig. 6(a) and (b)) produced the
334 highest power savings. For example, increasing the superheated refrigerant temperature in the heat source
335 from 75 to 100° C increased energy savings for R1234yf and R1234zeE by 21 to 30.5% and 17 to 25%,
336 respectively. However, the energy savings from refrigerants R1270 and R161 depend on the condenser
337 temperature and only produce positive energy savings when the thermal store temperatures exceed a
338 threshold of 85°C and 95°C, respectively.

339

340 **5.2.3 Effect of thermal store temperature on thermal compressor and condenser heat duties**

341 The amount of heat transfer to the refrigerant vapour in the thermal compressor is contingent on the
342 refrigerant type, the temperature of the refrigerant entering the thermal compressor, and the condenser
343 temperature. Fig. 7 shows that, for a given condenser temperature, the use of R1234yf and R1234zeE
344 affords higher heat supply from the heat source across the range of temperatures considered. For example,
345 at condenser temperature of 65°C and thermal store temperature of 100°C, the amount of heat transfer is
346 1.5 and 1.2 kW for R1234yf and R1234zeE respectively as shown in Fig. 7(a) and (b). In contrast, the heat
347 transfer from the thermal store when using refrigerant R1270 and R161 is only possible if the thermal store
348 temperature is above a certain threshold. For example, at condenser temperature of 60°C, the thermal store
349 temperature needs to be above 80°C and 85°C when using R1270 and R161 respectively for the thermal
350 compressor to operate, as shown in Fig. 7(c) and (d). However, this contributes to increasing the heat
351 rejection load imposed on the condenser by as much as 100%, as shown in all cases of Fig. 7.

352

353 **5.2.4 Effect of thermal store temperature on the cycle compression ratio**

354 The mechanical compressor workload is related to the refrigerant pressure compression ratio (p_2/p_8). The
355 integration of thermal compressor bears part of the cooling load and so reduces the mechanical
356 compression ratio in the TMVC cycle to (p_2/p_1). For example, Fig. 8(a) and (b) illustrate that at a heat source
357 temperature of 100°C, and using R1234yf and R1234zeE refrigerants, the compression ratio is improved
358 by 37% and 33.5% respectively, for a condenser temperature of 65°C. On the other hand, using refrigerants
359 R1270 and R161 enhances the compression ratio only when the thermal store temperature exceeds 85°C
360 at a condenser temperature of 65°C. The pressure ratio enhancement shown in Fig 8(c) and (d) is
361 approximately 27% and 22% for R1270 and R161, respectively. The isentropic efficiency of the TMVC
362 mechanical compressor improves by 4% compared to the BVC at a condenser temperature of 65°C. This
363 enhancement is primarily due to the reduction of irreversibility associated with lower compression ratios.

364

365

366 **5.2.5 Effect of the ejector design efficiencies on the coefficient of performance**

367 The overall energy performance of the TMVC system is strongly influenced by the efficiency of the ejector
368 design, which accounts for friction losses in the nozzle, suction, mixing, and diffuser components. Fig. 9
369 illustrates the improvements in COP of the cycle when the efficiencies of the ejector nozzle, suction, mixing,
370 and diffuser parts are increased from 0.5 to 1 for the thermal compressor discharge temperature, T_s , of
371 95°C , a condenser temperature, T_{con} , of 65°C , and an evaporator temperature, T_{evp} , of 5°C .

372 As shown in Fig. 9(a), the refrigerant R1234yf achieved the highest COP increase (from 22.23% to 44.5%),
373 while R161 performed the least improvement (from 4.9% to 19.5%). For R161, particularly, if the ejector
374 nozzle efficiency is less than 0.8, the thermal compressor stage is by-passed because the discharge
375 refrigerant temperature is higher than that of the thermal store. This is indicated in Fig. 9 by a step change
376 improvement when the COP is above 0.8. Similar trends and ranges of COP improvement are also observed
377 when increasing the efficiency of the ejector diffuser and mixing components. Furthermore, it is noted that
378 the suction nozzle efficiency has a lesser impact on COP improvement, as shown in Fig. 9(b), where, for
379 example, the COP increased from 37.4% to 42% when using R1234yf refrigerant.

380

381 **5.2.6 Effect of the condenser temperature on the pressure lift**

382 The effect of condenser temperature variation on the ejector pressure lift (P_{11}/P_8) is illustrated in Fig. 10. As
383 the condenser temperature increases from 50°C to 65°C , the pressure lift increases for all refrigerant types,
384 which can subsequently enhance the system's overall COP. For example, R1234yf exhibits the most
385 significant improvement, with its pressure lift rising from 1.14 to 1.27. In contrast, R161 refrigerant shows a
386 more modest increase in pressure lift from 1.1 to 1.2 as the condenser temperature increases from 50°C to
387 65°C . This indicates that the adverse effect of high ambient temperature on traditional vapour compression
388 air conditioning systems efficiency is mitigated in the proposed TMVC system.

389

390

391

392 **Conclusion**

393

394 This paper presents a novel air conditioning system designed to improve the energy efficiency of the
395 traditional vapour compression cycle. This improvement is achieved by integrating an ejector device for
396 refrigerant expansion and incorporating a thermally driven second-stage constant volume compression
397 process, forming the proposed thermo-mechanical vapour compression (TMVC) cooling system. The study
398 also evaluates the energy performance of the system using low global warming potential (GWP) refrigerants
399 such as R1234yf, R1234zeE, R1270, and R161. The TMVC cooling system aims to improve the coefficient
400 of performance (COP) of the well-established conventional vapour compression technology, especially in
401 hot climates where air conditioning is used extensively to support thermal comfort in buildings.

402 The synergy between the abundant solar energy in hot climates and the demand for air conditioning makes
403 the system ideal candidate for the future development of solar assisted air conditioning systems. The main
404 findings of this study are summarised as follows:

405

- 406 i) The TMCV cycle, with refrigerants R1234yf and R1234zeE that have lower discharge
407 temperatures of 71.2°C and 73.6°C respectively, exhibited higher improvement in COP
408 of,42.7% and 33.4% respectively, higher energy saving of 30% and 25% at condenser
409 temperature of 60°C and thermal store temperature of 100°C.
- 410 ii) The proposed TMVC cycle achieves a COP range of 2 to 5 for the considered refrigerants and
411 given operating conditions of a condenser temperature of 55 to 65° C, an evaporator
412 temperature of 5° C, and a thermal store discharge temperature of 75 to 100° C.
- 413 iii) Compared to the basic vapor compression cycle, the TMVC demonstrates a COP improvement
414 of 26% to 44%, along with energy savings of 21% to 30%. These results were observed at a
415 condenser temperature of 65°C, with thermal store temperatures ranging from 75°C to 100°C,
416 using the R1234yf refrigerant.
- 417 iv) The thermal performance of the TMVC system remains unaffected by the condenser
418 temperature, a significant advantage for air conditioning systems in hot climates.

419 Future work should focus on the design, integration and evaluation of a solar thermal collector to reduce
420 the environmental impact of air conditioning systems and promote the adoption of renewable energy
421 systems. In addition, a full economic analysis should be conducted to establish the cost-effectiveness of the
422 proposed technology both for small and large-scale applications.

423

424

425 **Acknowledgment**

426 The authors would like to acknowledge “The Higher Committee for Education Development in Iraq” for
427 providing the financial support through a student scholarship.

428

429

430 **References:**

431 International Energy Agency, I. (2018). *The Future of Cooling Opportunities for energy-efficient air*
432 *conditioning Together Secure Sustainable*. www.iea.org/t&c/

433 Abd-Elhady, M. S., Bishara, E., & Halim, M. A. (2021). Increasing the Cooling Rate of the Vapor
434 Compression Cycle by Heating. *International Journal of Air-Conditioning and Refrigeration*,
435 29(1). <https://doi.org/10.1142/S2010132521500097>

436 Al-Sayyab, A. K. S., Navarro-Esbrí, J., Barragán-Cervera, A., Kim, S., & Mota-Babiloni, A. (2022).
437 Comprehensive experimental evaluation of R1234yf-based low GWP working fluids for
438 refrigeration and heat pumps. *Energy Conversion and Management*, 258.
439 <https://doi.org/10.1016/j.enconman.2022.115378>

440 Aranguren, P., Sánchez, D., Haida, M., Smolka, J., Cabello, R., Rodríguez, A., & Astrain, D. (2024).
441 Effect of thermoelectric subcooling on COP and energy consumption of a propane heat pump.
442 *Applied Thermal Engineering*, 257. <https://doi.org/10.1016/j.applthermaleng.2024.124242>

443 Bell, I. H., Wronski, J., Quoilin, S., & Lemort, V. (2014). Pure and pseudo-pure fluid thermophysical
444 property evaluation and the open-source thermophysical property library coolprop. *Industrial*
445 *and Engineering Chemistry Research*, 53(6), 2498–2508. <https://doi.org/10.1021/ie4033999>

446 Bellos, E., Vrachopoulos, M. G., & Tzivanidis, C. (2017). Energetic and exergetic investigation of a
447 novel solar assisted mechanical compression refrigeration system. *Energy Conversion and*
448 *Management*, 147, 1–18. <https://doi.org/10.1016/j.enconman.2017.05.040>

449 Bouraba, A., Saighi, M., Saidani-Scott, H., & Hamidat, A. (2017). Mécanisme de refroidissement
450 d'un conditionneur d'air solaire : étude basée sur le diagramme pression-enthalpie.

451 *International Journal of Refrigeration*, 80, 274–291.
452 <https://doi.org/10.1016/j.ijrefrig.2017.05.008>

453 Brunin, O., Feidt, M., & Hivet, B. (1997). Comparison of the working domains of some compression
454 heat pumps and a compression-absorption heat pump. In *IntJ. Refrig* (Vol. 20, Issue 97).

455 Cao, X., Liang, X., Shao, L., & Zhang, C. (2022). Performance analysis of an ejector-assisted two-
456 stage evaporation single-stage vapor-compression cycle. In *Applied Thermal Engineering* (Vol.
457 205). Elsevier Ltd. <https://doi.org/10.1016/j.applthermaleng.2021.118005>

458 Chen, Q., Yu, M., Yan, G., & Yu, J. (2022). Thermodynamic analyses of a modified ejector enhanced
459 dual temperature refrigeration cycle for domestic refrigerator/freezer application. *Energy*, 244.
460 <https://doi.org/10.1016/j.energy.2021.122565>

461 de Paula, C. H., Duarte, W. M., Rocha, T. T. M., de Oliveira, R. N., & Maia, A. A. T. (2020). Optimal
462 design and environmental, energy and exergy analysis of a vapor compression refrigeration
463 system using R290, R1234yf, and R744 as alternatives to replace R134a. *International Journal*
464 *of Refrigeration*, 113, 10–20. <https://doi.org/10.1016/j.ijrefrig.2020.01.012>

465 Elhelw, M., El-Maghlany, W. M., & Abdelaziz, A. H. (2022). Experimental and theoretical study of
466 hybrid electric solar driven vapour compression system. *Renewable Energy*, 182, 452–466.
467 <https://doi.org/10.1016/j.renene.2021.10.035>

468 Ersoy, H. K., & Bilir Sag, N. (2014). Preliminary experimental results on the R134a refrigeration
469 system using a two-phase ejector as an expander. *International Journal of Refrigeration*, 43,
470 97–110. <https://doi.org/10.1016/j.ijrefrig.2014.04.006>

471 Jain, V., Khurana, S., Parinam, A., Sachdeva, G., Goel, A., & Mudgil, K. (2024). Experimental analysis
472 of an ejector assisted dual-evaporator vapor compression system. *Energy Conversion and*
473 *Management*, 300. <https://doi.org/10.1016/j.enconman.2023.117966>

474 *Kigali amendment to the montreal Protocol: A Crucial Step in the Fight Against Catastrophic*
475 *Climate Change*. (2016).

476 Kulkarni, S., Chavali, S., & Dikshit, S. (2023). A review on analysis of Vapour Compression
477 Refrigeration System (VCRS) for its performance using different ecofriendly refrigerants and
478 nanofluids. *Materials Today: Proceedings*, 72, 878–883.
479 <https://doi.org/10.1016/j.matpr.2022.09.085>

480 Kwan, T. H., Shen, Y., Wu, Z., & Yao, Q. (2020). Performance analysis of the thermoelectric device as
481 the internal heat exchanger of the trans-critical carbon dioxide cycle. *Energy Conversion and*
482 *Management*, 208. <https://doi.org/10.1016/j.enconman.2020.112585>

483 Li, H., Cao, F., Bu, X., Wang, L., & Wang, X. (2014). Performance characteristics of R1234yf ejector-
484 expansion refrigeration cycle. *Applied Energy*, 121, 96–103.
485 <https://doi.org/10.1016/j.apenergy.2014.01.079>

486 Özgür, A. E., Kabul, A., & Kizilkan, Ö. (2014). Exergy analysis of refrigeration systems using an
487 alternative refrigerant (HFO-1234yF) to R-134a. *International Journal of Low-Carbon*
488 *Technologies*, 9(1), 56–62. <https://doi.org/10.1093/ijlct/cts054>

489 Rajendran, P., Narayanaswamy, G. R., & Dhasan, M. L. (2019). Tuning thermostatic expansion valve
490 for implementing suction line heat exchanger in mobile air conditioning system. *Journal of the*
491 *Brazilian Society of Mechanical Sciences and Engineering*, 41(4).
492 <https://doi.org/10.1007/s40430-019-1680-4>

493 Riahi, A., & Shafii, M. B. (2023). Parametric study of a vapor compression refrigeration system
494 integrated with a PCM storage tank for increasing condenser sub-cooled temperature. *Case*
495 *Studies in Thermal Engineering*, 47. <https://doi.org/10.1016/j.csite.2023.103100>

496 Riahi, A., & Shafii, M. B. (2024). Dynamic evaluation of a vapor compression refrigeration cycle
497 combined with a PCM storage tank for improving condenser performance. *Heliyon*, 10(16),
498 e35837. <https://doi.org/10.1016/j.heliyon.2024.e35837>

499 Sarkar, J. (2010). Geometric parameter optimization of ejector-expansion refrigeration cycle with
500 natural refrigerants. *International Journal of Energy Research*, 34(1), 84–94.
501 <https://doi.org/10.1002/er.1558>

502 Staubach, D., Michel, B., & Revellin, R. (2023). Refrigerant selection from an economic and TEWI
503 analysis of cascade refrigeration systems in Europe based on annual weather data. *Applied*
504 *Thermal Engineering*, 230. <https://doi.org/10.1016/j.applthermaleng.2023.120747>

505 Utage, A. S., Mali, K. V., & Phadake, H. C. (2021). Performance simulation of HFC-161 as an
506 alternative refrigerant to HCFC-22 for room air conditioner. *Materials Today: Proceedings*, 47,
507 5594–5597. <https://doi.org/10.1016/j.matpr.2021.03.474>

508 Wang, F., & You, T. (2023). Comparative analysis on the life cycle climate performance of ground
509 source heat pump using alternative refrigerants. *Case Studies in Thermal Engineering*, 42.
510 <https://doi.org/10.1016/j.csite.2023.102761>

511 Yıldız, G., Gürel, A. E., Ceylan, İ., Ergün, A., Karaağaç, M. O., & Ağbulut, Ü. (2023). Thermodynamic
512 analyses of a novel hybrid photovoltaic-thermal (PV/T) module assisted vapor compression
513 refrigeration system. *Journal of Building Engineering*, 64.
514 <https://doi.org/10.1016/j.jobbe.2022.105621>

515 Zarei, A., Elahi, S., & Pahangeh, H. (2022). Design and analysis of a novel solar compression-ejector
516 cooling system with eco-friendly refrigerants using hybrid photovoltaic thermal (PVT) collector.
517 *Thermal Science and Engineering Progress*, 32. <https://doi.org/10.1016/j.tsep.2022.101311>

518 Zhang, Z., Feng, X., Tian, D., Yang, J., & Chang, L. (2020). Progress in ejector-expansion vapor
519 compression refrigeration and heat pump systems. In *Energy Conversion and Management*
520 (Vol. 207). Elsevier Ltd. <https://doi.org/10.1016/j.enconman.2020.112529>

521

522

523

524

525 **Table 1** The characteristics of the selected refrigerants

Refrigerant	Boiling Temperature (°C)	Critical temperature (°C)	Critical pressure (kPa)	Latent heat evaporation (kJ/kg)	Safety Group	ODP	GWP	Reference
R134a	-26.3	101.1	4,059.2	198.17	A1	0	1370	(Wang & You, 2023)
R410A	-51.4	70.5	4,901.2	221.57	A2L	0	2100	(Utage et al., 2021)
R1234yf	-19	94.7	3,382.2	163.3	A2L	0	<1	(Wang & You, 2023)
R1234zeE	-37.1	109.4	3,634.9	184.27	A2L	0	<1	(Wang & You, 2023)
R161	-37.6	102.2	5,010	379.2	A3	0	12	(Utage et al., 2021)
R1270	-47.7	91.1	4,555	377.81	A3	0	2	(Staubach et al., 2023)

526

527

528 **Table 2** Basic vapour compression cycle design parameters (Özgür et al., 2014).

Key parameter	Equation
Compressor work	$W_{comp,BVC} = (h_{2'} - h_8)$ (1)
Cooling capacity	$Q_{ev,BVC} = (h_8 - h_{7'})$ (2)
Condenser heat rejection	$Q_{con,BVC} = (h_{2'} - h_4)$ (3)
COP	$COP_{BVC} = \frac{Q_{ev,BVC}}{W_{comp,BVC}} = \frac{h_8 - h_{7'}}{h_{2'} - h_8}$ (4)
Volumetric cooling capacity	$VCC_{BVC} = \frac{(h_8 - h_{7'})}{v_8}$ (5)

529

530

531

532

533

534

535 **Table 3** TMVC thermodynamic cycle refrigerant properties

Thermodynamic state	Refrigerant Property	Relationship	Eq
Condenser discharge line (Point 4)	Pressure	$P_4 = P_{con} = P(T_{con}, x_4 = 0)$	(6)
	Enthalpy	$h_4 = h(P_{con}, T_{sub})$	(7)
	entropy	$S_4 = s(P_{con}, T_{sub})$	(8)
Ejector discharge (isentropic expansion process) (point 5)	Pressure	$P_5 = P_9$	(9)
	Enthalpy (isentropic)	$h_{5,is} = h(P_5, S_5)$	(10)
	Entropy	$S_4 = S_5$	(11)
	Enthalpy (actual)	$h_5 = h_4 + \eta_{mn}(h_{5,is} - h_4)$	(12)
	Refrigerant velocity	$V_{mn} = \sqrt{2(h_4 - h_5)}$	(13)
Separator liquid line (Point 6)	Enthalpy	$h_6 = h(P_{11}, x = 0)$	(14)
Evaporator inlet (Point 7)	Enthalpy	$h_7 = h_6$	(15)
Ejector suction line (point 8)	Pressure	$P_8 = P_{evp} = P(T_{evp}, x = 1)$	(16)
	Enthalpy	$h_8 = h(T_{evp}, x = 1)$	(17)
	entropy	$S_8 = s(T_{evp}, x = 1)$	(18)
Ejector suction chamber (isentropic process) (point 9)	Entropy	$S_9 = S_8$	(19)
	Enthalpy	$h_{9,is} = h(P_9, S_5)$	(20)
	Enthalpy (actual)	$h_9 = h_8 + \eta_{sn}(h_{9,is} - h_8)$	(21)
	Refrigerant Velocity	$V_{sn} = \sqrt{2(h_8 - h_9)}$	(22)
Constant area of the ejector (point 10)	Enthalpy	$h_{10} = r(h_5 + \frac{V_{mn}^2}{2}) + (1 - r)(h_8 + \frac{V_{sn}^2}{2})$	(23)
	entropy	$- 0.5V_{mix}^2$	(24)
Ejector diffuser exit Point (11)	Pressure	$S_{10} = S(h_{10}, P_{10})$	(25)
	Enthalpy	$P_{11} = P(S_{10}, h_{11,is})$	(26)
	enthalpy	$h_{11} = h_{10} + 0.5V_{mix}^2$	(27)
	entropy	$h_{11,is} = h_{10} + \eta_{diff}(0.5V_{mix}^2)$	(28)
	Vapour quality	$S_{10} = S_{11}$	(29)
Compressor suction line (Point 1)	Enthalpy	$x_{11} = x(p_{11}, h_{11}), x_{11} = \frac{\dot{m}_{con}}{\dot{m}_{con} + \dot{m}_{ev}}$	(30)
Compressor discharge line (Point 2)	Enthalpy	$h_1 = h(P_{11}, T_{sup})$	(31)
		$h_2 = h_1 + \frac{(h_{2,is} - h_1)}{\eta_{is}}$	(32)
Thermal store vapour line (Point 3)	Specific volume	$h_{2,is} = h(P_2, S_1)$	(33)
	Enthalpy	$v_3 = v_2, v_3 = v(P_{con}, T_s)$	(34)
	temperature	$h_3 = h(P_{con}, v_3)$	(35)
		$T_{3'} = T(P_C, h_{3'})$	(35)
		$T_3 = T_s$	

536

537

538 **Table 4.** Comparison of theoretical and experimental results of the ejector cooling system

Case No.	Cooling Capacity (kW)	Theoretical COP (Present work)	Experimental COP (Ersoy & Bilir Sag, 2014)	% Deviation
Case #1	4.2	2.5	2.393	+4.28
Case #2	4.36	2.31	2.23	+3.46
Case #3	4.47	2.36	2.13	+9.75

539

540

541 **Table 5_**Comparison of experimental results by (Elhelw et al., 2022) and proposed computer model

Refrigerant state	Description	Experiment (Elhelw et al., 2022)			Computer model			
		Temperature (°C)	Pressure (bar)	Enthalpy (kJ/kg)	Pressure (bar)	Deviation (%)	Enthalpy (kJ/kg)	Deviation (%)
1	Mechanical Compressor Suction	6.46	3.13	402.14	3.14	-0.32	403.66	-0.38
2	Mechanical Compressor discharge	28.37	5.83	416.35	6.7	-14.9	422.78	-1.5
3	Thermal Compressor discharge	104.26	9.57	489.39	8.9	+6.17	488.61	+0.16
4	Subcooled condenser discharge	30.74	9.36	243.48	8.98	+4.06	242.57	+0.37
5	Evaporator inlet	2.15	3.15	243.16	3.14	+0.32	242.57	+0.24

542

543

544 **Table 6** TMVC design parameters

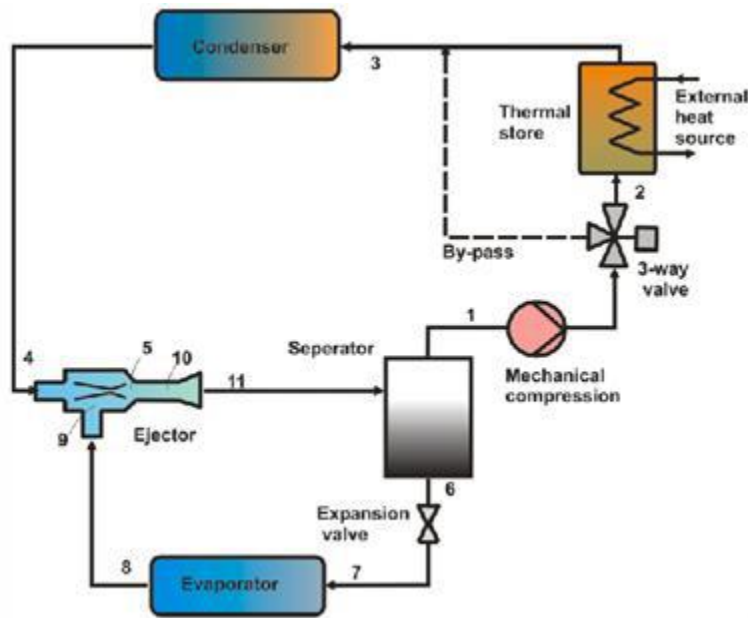
Parameters	Value	545
Condenser temperature	55° C to 65° C	
Evaporator temperature	5° C	546
Superheated temperature	5° C	
Subcooled temperature	5° C	547
Ejector suction nozzle pressure drop	20 kPa	
Mechanical compressor efficiency	0.8	548
Thermal compressor discharge temperature	75 °C to 100 °C	
Cooling capacity	3,517 W	549

550

551 **Table 7** Basic Vapour Compression (BVC) cycle results ($T_{con}= 65^{\circ}\text{C}$ and $T_{evp}=5^{\circ}\text{C}$)

Operating parameter	Critical temperature ($^{\circ}\text{C}$)	Discharge Temperature ($^{\circ}\text{C}$)	Compressor work (kW)	Condenser heat capacity (kW)	Volumetric cooling capacity (kJ/Kg)	Refrigerant mass flow rate (kg/s)	COP (-)
R134a	101.1	82.4	1.66	4.85	1974	0.030	2.12
R410A	70.5	124.7	1.91	5.04	4230	0.029	1.85
R1234yf	94.7	71.2	1.81	4.97	1731	0.041	1.94
R1234zeE	109.4	73.6	1.68	4.86	1455	0.033	2.10
R161	102.2	98.8	1.58	4.78	2894	0.014	2.22
R1270	91.1	88.2	1.69	4.87	3119	0.016	2.08

552



553

554

555

Fig 1. Schematic diagram of the TMVC system

556

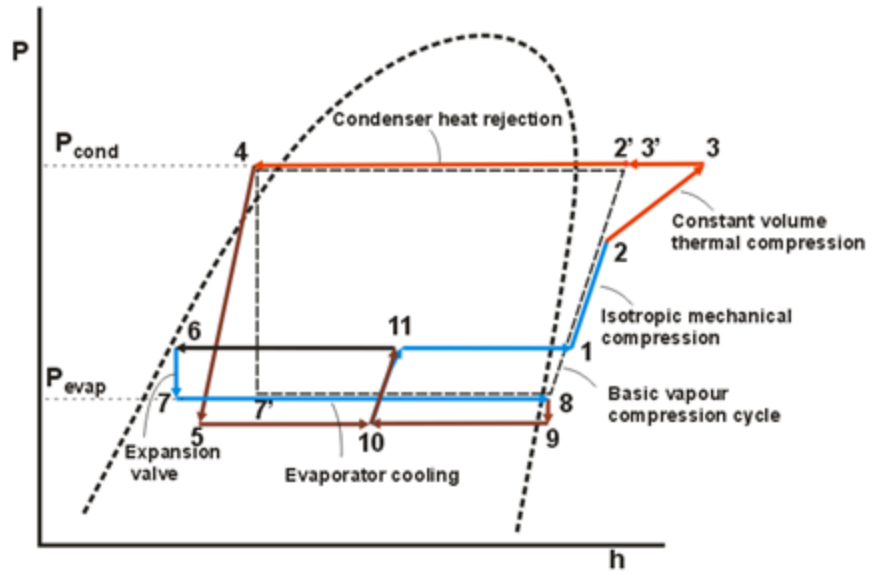
557

558

559

560

561



562

563

564

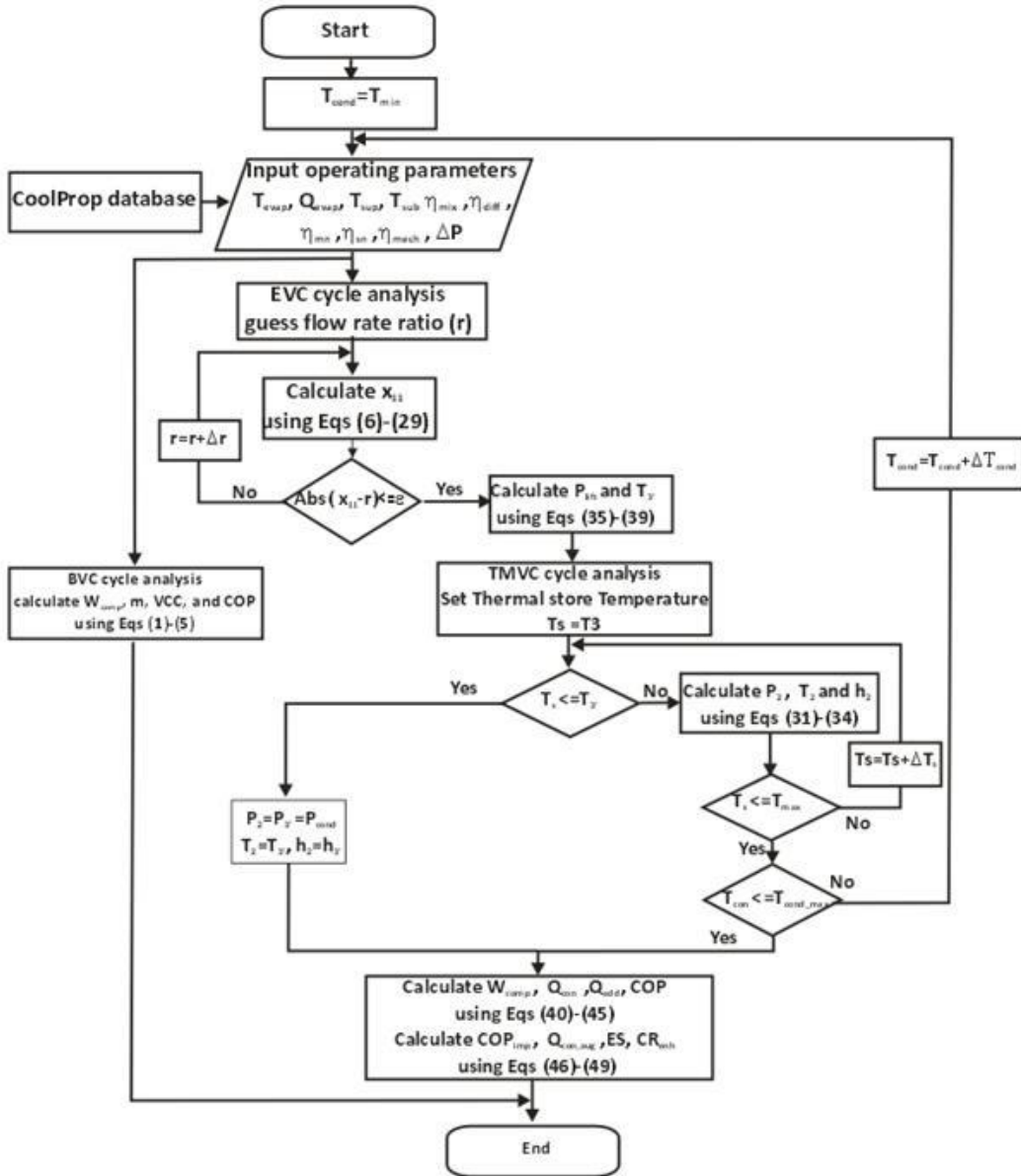
Fig. 2. TMVC system p-h thermodynamic cycle

565

566

567

568



569

570

571

Fig. 3 Flow chart of the computational algorithm

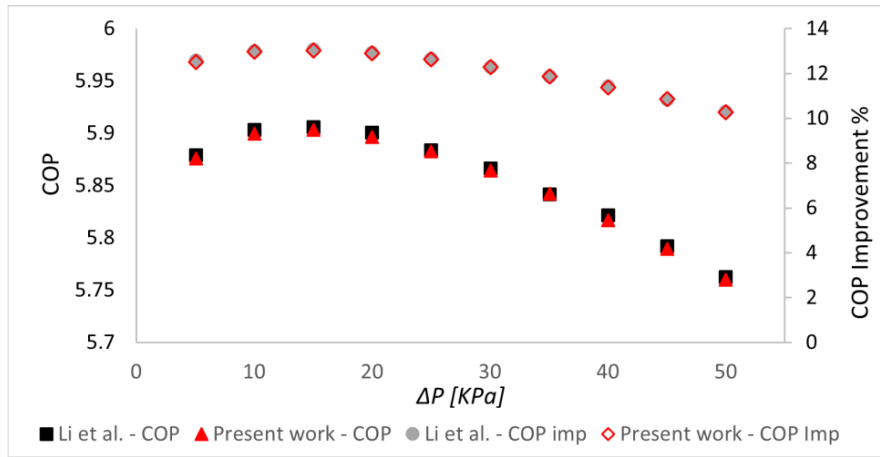
572

573

574

575

576



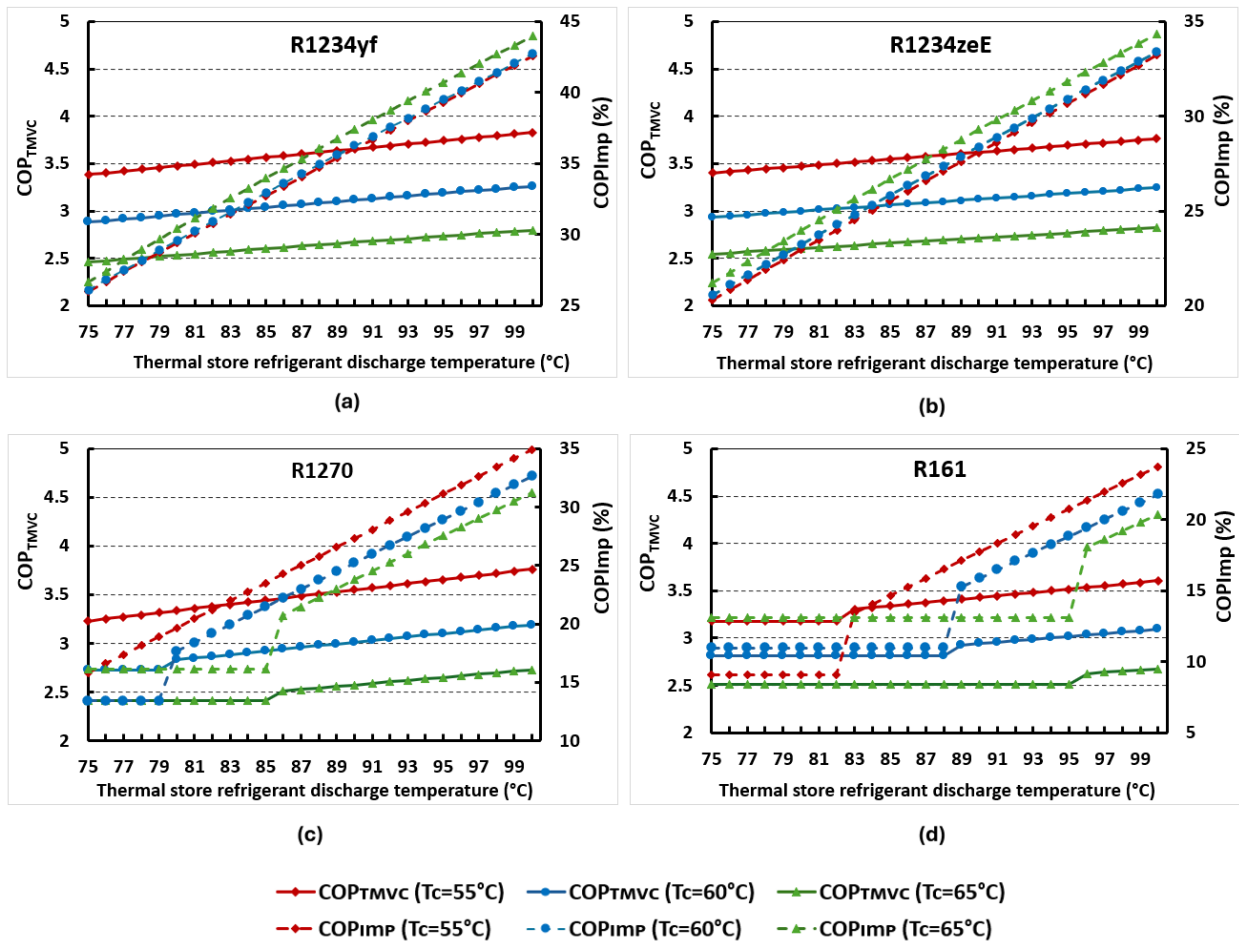
577

578

579

Fig. 4 Data validation of present work with Li et al. (2014)

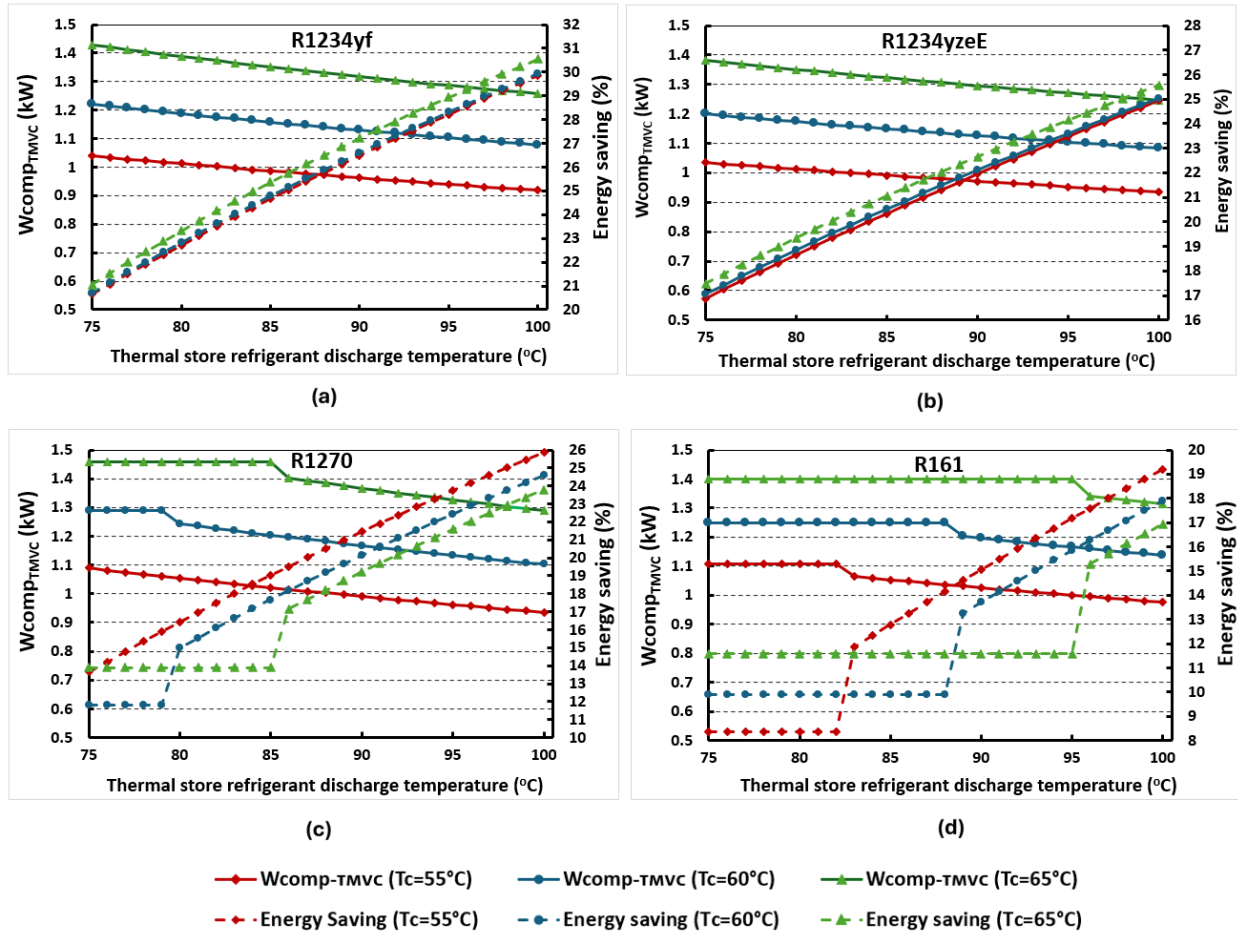
580



581

582

Fig. 5 Effect of thermal store temperature on COP a) R1234yf, b) R1234zeE, c) R1270 and d) R161



583

584

585 **Fig. 6** Effect of thermal store temperature on compressor work and energy saving a) R1234yf,

586

b) R1234zeE, c) R1270 and d) R161

587

588

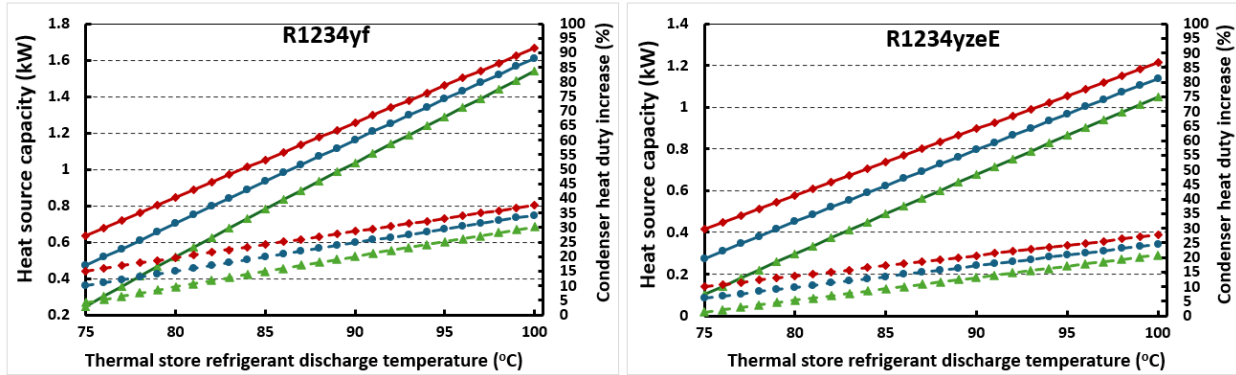
589

590

591

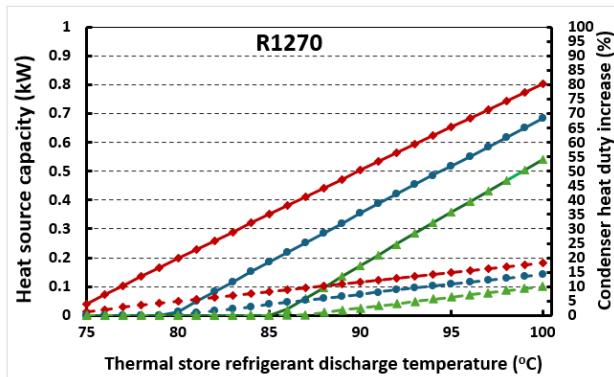
592

593

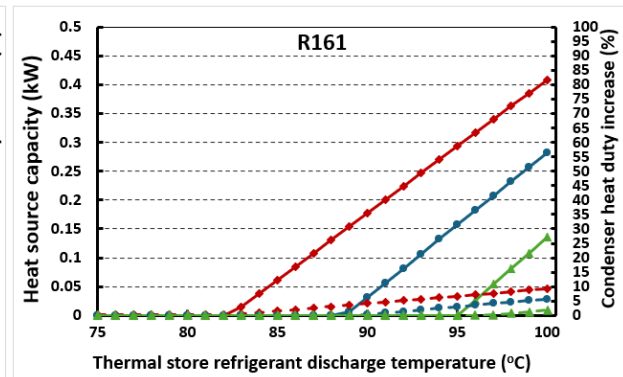


(a)

(b)



(c)



(d)

◆ Heat cap (Tc=55°C)
 ● Heat cap (Tc=60°C)
 ▲ heat cap (Tc=65°C)
◆ Cond duty (Tc=55°C)
 ● Cond duty (Tc=60°C)
 ▲ Cond duty (Tc=65°C)

594

595

596 **Fig. 7** Effect of thermal store temperature on heat source capacity and condenser heat duty. a)

597

R1234yf, b) R1234zeE, c) R1270 and d) R161

598

599

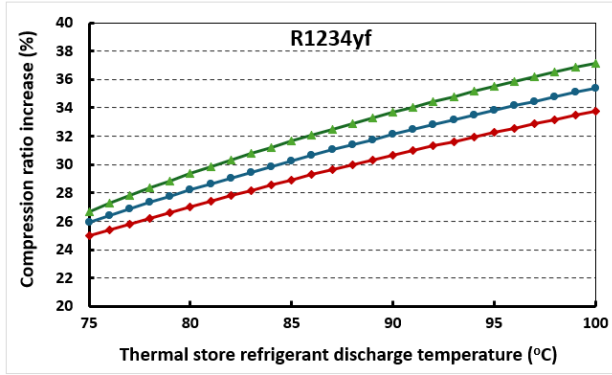
600

601

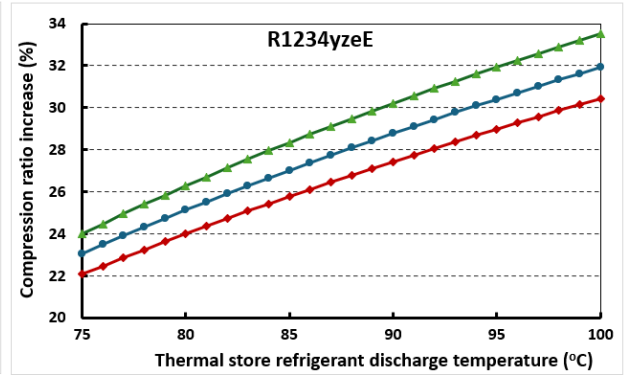
602

603

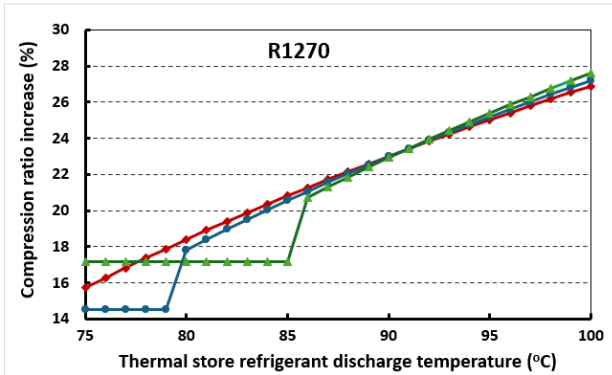
604



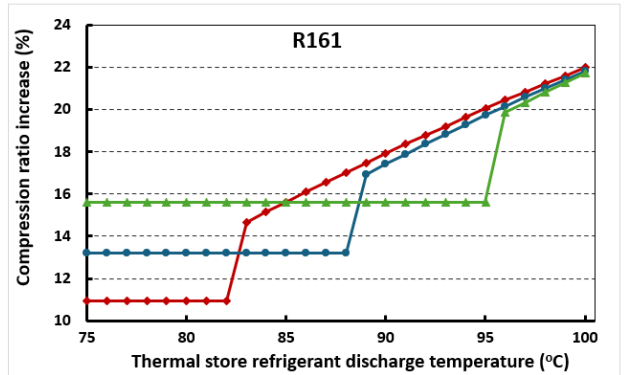
(a)



(b)



(c)



(d)

—◆— Tc=55°C —●— Tc=60°C —▲— Tc=65°C

605

606

607 **Fig. 8** TMVC cycle compression ratio increase a) R1234yf, b) R1234zeE, c) R1270 and d) R161

608

609

610

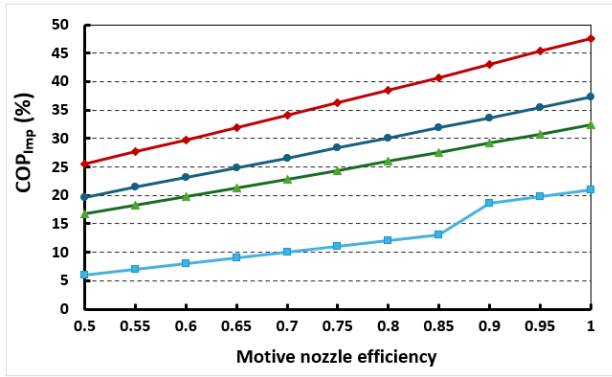
611

612

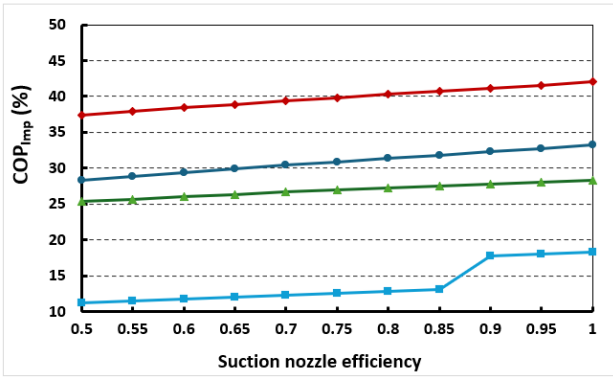
613

614

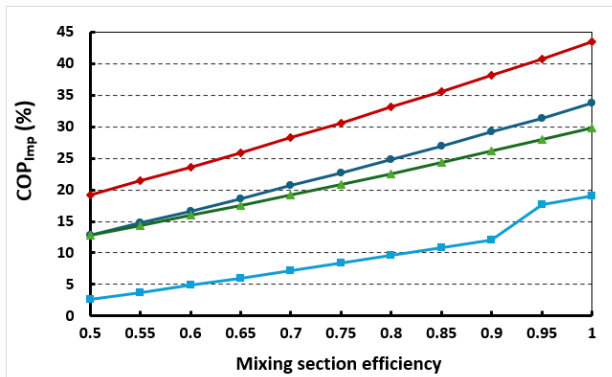
615



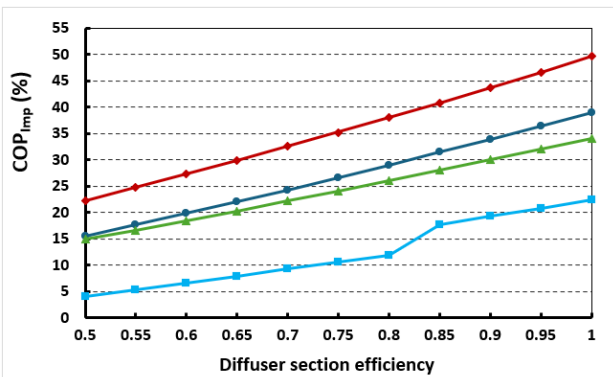
(a)



(b)



(c)



(d)

—●— R1234yf —●— R1234zeE —▲— R1270 —■— R161

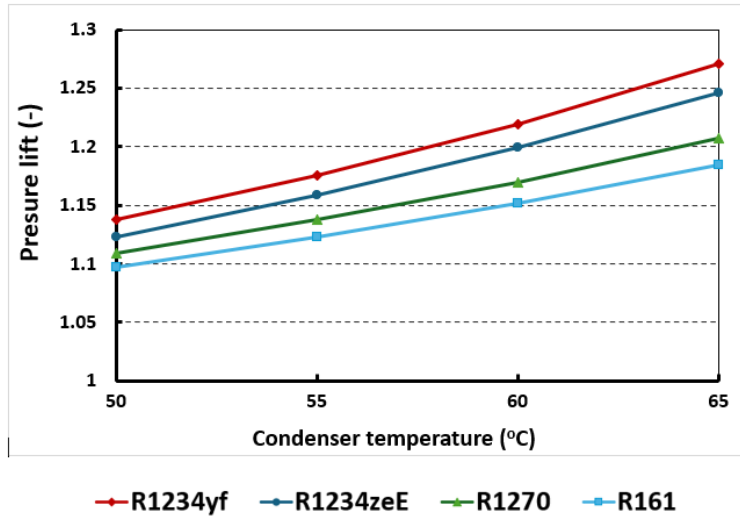
616

617

618

Fig. 9 Effect of the ejector component efficiencies

619



620

621

622

Fig. 10 Ejector pressure lift